energies

MDPI

Article

Co-Optimization of CO_2 Storage and Enhanced Gas Recovery Using Carbonated Water and Supercritical CO_2

Abdirizak Omar, Mouadh Addassi, Volker Vahrenkamp and Hussein Hoteit *

Physical Science and Engineering Division (PSE), King Abdullah University of Science and Technology, Thuwal, Jeddah 23955, Saudi Arabia; abdirizakali.omar@kaust.edu.sa (A.O.); mouadh.addassi@kaust.edu.sa (M.A.); volker.vahrenkamp@kaust.edu.sa (V.V.)
* Correspondence: hussein.hoteit@kaust.edu.sa

Abstract: CO_2-based enhanced gas recovery (EGR) is an appealing method with the dual benefit of improving recovery from mature gas reservoirs and storing CO_2 in the subsurface, thereby reducing net emissions. However, CO_2 injection for EGR has the drawback of excessive mixing with the methane gas, therefore, reducing the quality of gas produced and leading to an early breakthrough of CO_2. Although this issue has been identified as a major obstacle in CO_2-based EGR, few strategies have been suggested to mitigate this problem. We propose a novel hybrid EGR method that involves the injection of a slug of carbonated water before beginning CO_2 injection. While still ensuring CO_2 storage, carbonated water hinders CO_2-methane mixing and reduces CO_2 mobility, therefore delaying breakthrough. We use reservoir simulation to assess the feasibility and benefit of the proposed method. Through a structured design of experiments (DoE) framework, we perform sensitivity analysis, uncertainty assessment, and optimization to identify the ideal operation and transition conditions. Results show that the proposed method only requires a small amount of carbonated water injected up to 3% pore volumes. This EGR scheme is mainly influenced by the heterogeneity of the reservoir, slug volume injected, and production rates. Through Monte Carlo simulations, we demonstrate that high recovery factors and storage ratios can be achieved while keeping recycled CO_2 ratios low.

Keywords: CCUS; CO_2 storage; enhanced gas recovery; carbonated water; optimization

Citation: Omar, A.; Addassi, M.; Vahrenkamp, V.; Hoteit, H. Co-Optimization of CO_2 Storage and Enhanced Gas Recovery Using Carbonated Water and Supercritical CO_2. *Energies* **2021**, *14*, 7495. https://doi.org/10.3390/en14227495

Academic Editors: Marko Cvetković, Iva Kolenković Močilac and João Fernando Pereira Gomes

Received: 4 September 2021
Accepted: 28 October 2021
Published: 10 November 2021

1. Introduction

The global demand for energy has been rising over the past few decades and is expected to continue growing. In 2021 alone, this demand is projected to increase by approximately 4.6% [1]. Expanding industries and the world's continuously growing population are major contributors to the global thirst for energy [2]. Despite significant advancements in renewable energy technologies, fossil fuels still remain the dominant source of world energy, and this trend is predicted to continue [3–5]. Currently, oil, natural gas, and coal contribute more than 70% of primary energy consumed globally [6]. However, a preference for natural gas is becoming evident, as it is considered a relatively cleaner source of energy. The share of natural gas as a source of global primary energy has risen from approximately 21% to 25% over the last decade, while comparatively, the shares of oil and coal have dropped [7]. This suggests that natural gas is expected to play a significant role in the global energy mix, especially for power generation and other important processes such as water desalination [8–10].

In contrast to the rise in demand for natural gas, the discovery of new conventional gas reservoirs has been decreasing. The global reserves-to-production ratio of natural gas has gradually declined over the last two decades [7]. Easily recoverable gas has become more difficult to find, yet the demand for it continues to rise. Therefore, it is crucial to improve the recovery from existing reservoirs, which can be achieved through enhanced gas recovery (EGR) processes [11,12].

On the other hand, the consumption of natural gas for energy contributes to greenhouse gas emissions. In 2020 in the United States, natural gas contributed to 34% of the energy consumed and 36% of the emitted carbon dioxide (CO_2) [13]. The world is currently striving to move to a net-zero carbon economy, and mitigating CO_2 emissions is an important step to this goal [14]. The use of CO_2 for EGR is an appealing solution with a dual benefit. First, CO_2 is disposed of in deep depleted gas reservoirs, which have a proven capacity to hold large amounts of gas for long periods of time, and second, an incremental amount of natural gas is recovered, which can help to offset the cost of CO_2 storage [12,15,16].

EGR involves the injection of a fluid that was not initially present in the gas reservoir to improve recovery. The most common EGR mechanism is gas–gas displacement, which has been widely studied both experimentally and numerically, and has been suggested as a way to prolong the life of gas reservoirs and improve recovery [11,17–19]. Gas injection helps to improve recovery via two main mechanisms: pressure maintenance, by replacing the produced methane [20,21], and by displacing the in-situ natural gas towards the production wells [11]. Gases that could be injected into the reservoirs for EGR include nitrogen and CO_2 [11,16]. While nitrogen serves as a viable fluid for EGR, particular emphasis has been placed on CO_2 because of the pressing need to reduce carbon emissions [22].

CO_2-based EGR is promising in terms of improving gas recovery and storing CO_2. When CO_2 is injected into gas reservoirs at elevated pressures and temperatures, it is relatively denser and more viscous than the in-situ gas. This change in the thermodynamic properties of CO_2 helps to achieve a better displacement efficiency [23]. However, the efficiency of this displacement is affected by the mixing of CO_2 and methane. Despite their density and viscosity contrasts, these two components are miscible at reservoir conditions [22]. Their miscibility is driven by mechanical mixing, dispersion, and molecular diffusion [18,24–27]. A major problem caused by this mixing is the early breakthrough of CO_2 to the production wells [19,28,29]. This mechanism is undesired as it leads to poor gas recovery efficiency due to excessive CO_2 recycling and gas contamination [23]. Furthermore, greater costs are incurred in separating the recycled CO_2 from the natural gas stream, leading to higher project CAPEX and OPEX associated with surface separation and processing facilities [22,30]. Because of the higher density of CO_2, density-driven dynamics take place leading to the down-dip flow of the heavier fluid [31–33]. The presence of thief layers or fractures at the bottom of the reservoir aggravates the problem as it can accelerate the injected fluid breakthrough [34,35].

While mixing, early breakthrough, and consequently, excess recycling of CO_2 have been identified as major obstacles in implementing CO_2-EGR, there has been little research done on strategies to mitigate these phenomena. Furthermore, studies on the co-optimization of CO_2-EGR and CO_2 storage are scarce in the literature, and the available studies approach the problem from a deterministic point of view. In this study, we propose a new CO_2-based EGR method that involves two stages. This EGR method is applicable for depleted gas reservoirs that have undergone the primary recovery stage. Such reservoirs are generally at low pressures ranging from 2000–5000 kPa [12]. When pure CO_2 is injected at these pressures, it will be in the gas phase, and this will result in prominent mixing and poor sweep and displacement efficiencies. Furthermore, the CO_2 mobility will be high leading to faster breakthrough and more recycling.

In our method, we propose to co-inject carbonated water and supercritical CO_2. The first stage involves the injection of a slug of carbonated water. This serves two main purposes. First, the injection of carbonated water helps to build up the pressure before beginning supercritical CO_2 injection. Second, CO_2 is disposed of in the aqueous phase, in which it is stable and exhibits increasing solubility as the pressure builds up. Furthermore, the presence of carbonated water, which is dense and flows down-dip to the bottom of the reservoir, inhibits the mobility of free CO_2. After a determined pore-volume of carbonated water is injected, the second stage begins. In this stage, pure CO_2 is injected in its supercritical state. At the relatively higher reservoir pressure, CO_2 has a better sweep

and displacement efficiency, and its mobility is inhibited due to the presence of carbonated water, therefore delaying breakthrough and reducing recycling.

In this work, we demonstrate the effectiveness of the proposed CO_2-based EGR method using reservoir simulation on a synthetic case and a real gas field. Furthermore, we perform a rigorous sensitivity analysis and uncertainty assessment to identify important uncertain and operation parameters that influence the processes under study. We also carry out optimization to identify the ideal operation and transition conditions considering methane recovery factor, CO_2 stored, and CO_2 recycled as our objective functions. These objective functions are coupled in a global objective function which is maximized to co-optimize between methane recovery and CO_2 storage. The sensitivity analysis, uncertainty assessment, and optimization are carried out as part of a structured Design of Experiments (DoE) framework that approaches the problem in a non-deterministic manner.

This paper is organized as follows. We first review the governing equations of multiphase fluid flow in porous media. The reservoir models are then introduced, followed by the proposed modeling workflow using a DoE. In the Results section, the thermodynamics of CO_2/water systems corresponding to CO_2 solubility and phase behavior is validated with measured data. The optimization approach is then applied for a synthetic case and a 3D field case. Finally, we provide the main conclusions.

2. Governing Equations

2.1. Flow Model

The governing equations for multiphase compositional flow in porous media are given by the component balance equations, Darcy's law, and the thermodynamic equilibrium between the phases [36]. In this work, we neglect capillary pressure due to the negligible interfacial tension in CO_2-methane systems at the conditions of interest in this study [37].

The material balance for each component in the phases is given by:

$$\phi \frac{\partial c z_i}{\partial t} + \nabla \cdot \mathbf{U}_i = 0 \qquad i = 1, \ldots, n_c \tag{1}$$

where ϕ is the porosity, c is the overall molar density, z_i is the overall mole fraction of component i, $\mathbf{U}_i$ is the molar flux of component i, and n_c is the total number of components. The molar flux $\mathbf{U}_i$ is given by:

$$\mathbf{U}_i = \sum_{\alpha} (c_\alpha x_{i,\alpha} \mathbf{v}_\alpha + S_\alpha \mathbf{J}_{i,\alpha}) \tag{2}$$

where α is the phase (water, oil, or gas), c_α is the molar density of phase α, $x_{i,\alpha}$ is the mole fraction of component i in phase α, $\mathbf{v}_\alpha$ is the phase velocity, S_α is the saturation of phase α, and $\mathbf{J}_{i,\alpha}$ is the diffusion flux of component i in phase α.

The global and phase compositions z_i and $x_{i,\alpha}$ respectively are constrained by the relation:

$$\sum_{i=1}^{n_c} z_i = \sum_{i=1}^{n_c} x_{i,\alpha} = 1 \tag{3}$$

The velocity of each phase is given by Darcy's law [38] as:

$$\mathbf{v}_\alpha = -\frac{\mathbf{k} k_{r,\alpha}}{\mu_\alpha} (\nabla p - \rho_\alpha \mathbf{g}) \tag{4}$$

where $\mathbf{k}$ is the absolute permeability of the porous medium, $k_{r,\alpha}$, μ_α, and ρ_α are the relative permeability, viscosity, and mass density respectively of phase α. p is the pressure and $\mathbf{g}$ is the gravitational acceleration vector.

The diffusion flux $\mathbf{J}$ is given by the generalized Fick's law [36,39]:

$$\mathbf{J}_\alpha = -c_\alpha \mathbf{D}_\alpha \nabla x_\alpha \tag{5}$$

where $\mathbf{D}_\alpha$ is the diffusion coefficient in phase α. For a multicomponent multiphase mixture, Equation (5) in an expanded form is given by:

$$\mathbf{J}_{i,\alpha} = -c_\alpha \sum_{j=1}^{n_c-1} \mathbf{D}_{i,j,\alpha} \nabla x_{j,\alpha}, \qquad i = 1, \ldots, n_c - 1 \tag{6}$$

The diffusion flux is constrained by [40]:

$$\sum_{i=1}^{n_c} \mathbf{J}_{i,\alpha} = 0 \tag{7}$$

The equation for pressure is written based on the concept of volume balance [41]:

$$\phi \xi \frac{\partial p}{\partial t} + \sum_{i=1}^{n_c} \overline{v}_i \nabla \cdot \mathbf{U}_i = 0 \tag{8}$$

where ξ is the total fluid compressibility and $\overline{v}_i$ is the total partial molar volume of component i.

The local thermodynamic equilibrium is defined by the equality of the fugacities of each component in the phases α_1 and α_2, that is:

$$f_{i,\alpha_1}(T, p, x_{j,\alpha_1}) = f_{i,\alpha_2}(T, p, x_{j,\alpha_2}), \quad i = 1, \ldots, n_c, \; j = 1, \ldots, n_c - 1 \tag{9}$$

In the above equation, $f_{i,\alpha}$ is the fugacity of a component i in phase α, which can be calculated using an equation of state.

2.2. CO_2-Water Phase Behavior

Understanding the interaction of CO_2 with water and the thermodynamic properties of the resulting mixture is an important part of CO_2 storage research. The dissolution of CO_2 in formation water is a primary CO_2 trapping mechanism over the long term. This reaction is relatively fast, and therefore, thermodynamic equilibrium is assumed. This equilibrium is expressed as the equality of fugacities in the gas and aqueous phases, such that:

$$f_{i,g} = f_{i,aq}, \quad i = 1, \ldots, n_c \tag{10}$$

where, $f_{i,g}$ is the fugacity of the ith component in the gas phase, and $f_{i,aq}$ is the fugacity of the ith component in the aqueous phase. For CO_2 gas, its fugacity in the gas phase is related to its partial pressure by:

$$f_{CO_2,g} = \varphi P_{CO_2} \tag{11}$$

where φ is the fugacity coefficient calculated from the Peng-Robinson EOS [42], and P_{CO_2} is the partial pressure of CO_2. In the aqueous phase, the fugacity of CO_2 is calculated using extended Henry's law [43].

$$f_{CO_2,aq} = y_{CO_2} H_{CO_2} \tag{12}$$

where, y_{CO_2} is the mole fraction of CO_2 in the aqueous phase and H_{CO_2} is Henry's constant. In pure water, Henry's constant in Equation (12) is calculated as a function of pressure, temperature, the universal gas constant, and partial molar volume with respect to a reference pressure, is given by:

$$\ln H_{CO_2} = \ln H^*_{CO_2} + \frac{\overline{v}_i (p - p^*)}{RT} \tag{13}$$

In saline water, a correction is made to Henry's constant to account for salinity, as follows:

$$\ln\left(\frac{H_{s,CO_2}}{H_{CO_2}}\right) = k_{s,CO_2} m_s \tag{14}$$

where H_{s,CO_2} is Henry's constant for CO_2 in the brine, H_{CO_2} is Henry's constant for CO_2 in pure water, k_{s,CO_2} is the Setchenov salting-out coefficient for a CO_2-water aqueous phase, and m_s is the molality of the dissolved salt.

3. Mechanistic Simulations

In this study, we use CMG GEM v2019.1, a commercial simulator from Computer Modeling Group (CMG). GEM is a fully-coupled compositional Equation of State (EOS) simulator capable of modeling subsurface flow problems, including CO_2 storage in oil and gas reservoirs [44].

3.1. Synthetic Reservoir 2D Cross-Section

We first consider a 2D gas reservoir model of physical dimensions $500 \times 10 \times 100$ m representing a vertical (I-K) cross-section. The cross-section is discretized into a $50 \times 1 \times 20$ regular Cartesian grid, as shown in Figure 1. There are 10 geological layers with varying permeability. Each layer is assumed to be homogenous, and the physical properties are uniform. The heterogeneity of the reservoir model is quantified by the Dykstra–Parsons coefficient [45], which is 0.5 for the case shown. There are two vertical wells (an injector and producer) completed across the entire thickness of the reservoir. Other physical, initialization, and sensitivity parameters for the simulation model are summarized in Appendix A, Table A1. The simulations of CO_2-EGR and storage for the synthetic reservoir cross-section are controlled by the constraints summarized in Table A2.

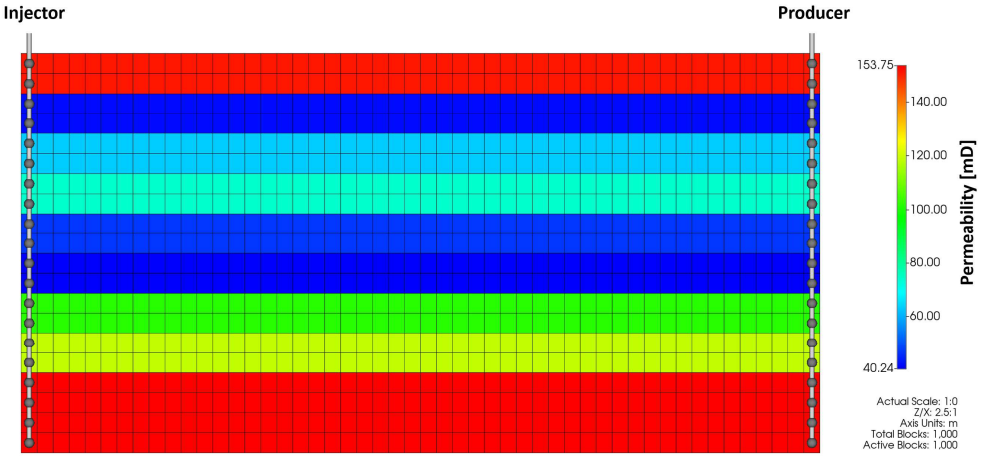

Figure 1. 2D synthetic reservoir cross-section showing the geologic layers, grid discretization, permeability distribution, and well completion.

For consistency, we define two dimensionless ratios that capture the production and injection rates and the pressure at which EGR has commenced. These ratios are defined as:

- **Productivity ratio**—is the ratio of the production rate to the injection rate.
- **Depletion pressure ratio**—is the ratio of the pressure at the start of EGR to the original reservoir pressure.

3.2. Real Reservoir 3D Sector

To demonstrate the proposed method in the presence of complex heterogeneities, we consider a 3D sector from a real gas field as shown in Figure 2. The sector is approximately $3500 \times 4100 \times 500$ ft in dimension and is discretized into a $63 \times 75 \times 32$ Cartesian grid, resulting in 151,200 grid blocks. The porosity varies between 0.05 and 0.23, while the permeability varies from less than 1 mD to more than 1600 mD. There is one vertical producer and one vertical injector. The producer is placed up-dip from the location of the injector. Relevant physical and initialization parameters are summarized in Table A3. Simulation constraints are presented in Table A4.

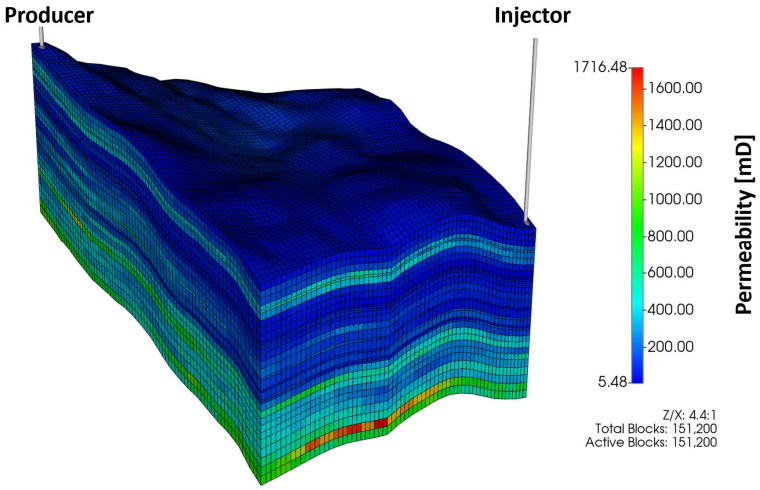

Figure 2. View of the 3D reservoir sector showing the permeability distribution and placement of the wells.

4. DoE Framework

We defined a Design of Experiments (DoE) workflow to perform sensitivity analysis, uncertainty assessment, and optimization. The key steps of this workflow are presented in Figure 3. We began by identifying and screening multiple possible uncertainty parameters. We used 2-level Plackett-Burman analysis [46,47] because it is computationally inexpensive [48]. However, in some cases, this design might not be enough to capture the response surface accurately. Therefore, we switched to Latin Hypercube Sampling (LHS). Using the experiments generated through LHS, we performed Sobol analysis [49] to identify the most sensitive parameters. These are the parameters considered for the uncertainty assessment. Furthermore, using the results of LHS sampling, we built a polynomial proxy model. We verified the quality of the proxy model using blind tests. Once the quality of the proxy model was verified, Monte Carlo simulations were performed using the proxy as part of the uncertainty assessment. We also performed optimization using the proxy model as part of the Latin Hypercube plus Proxy Optimization algorithm. The flowchart of the optimization algorithm is presented in Figure 4.

The proposed EGR method was evaluated based on 3 main dimensionless objective functions; methane recovery factor, CO_2 stored, and CO_2 recycled. These objective functions are defined as:

$$\text{Recovery Factor} = \frac{\text{CH}_4 \text{ mass produced}}{\text{CH}_4 \text{ mass originally in place}} \tag{15}$$

$$\text{CO}_2 \text{ Stored} = \frac{\text{CO}_2 \text{ mass injected} - \text{CO}_2 \text{ mass produced}}{\text{Maximum storable CO}_2 \text{ mass at target p, T}} \tag{16}$$

$$\text{CO}_2 \text{ Recycled} = \frac{\text{CO}_2 \text{ mass produced}}{\text{CO}_2 \text{ mass injected}} \tag{17}$$

These objective functions are coupled in a linear global objective function of the form $aX_1 + bX_2 - cX_3$, which is maximized to identify the ideal operation and transition conditions. The variables,X_1, X_2, and X_3 are the recovery factor, CO_2 stored, and CO_2 recycled respectively while a, b, and c are bios coefficients that could be varied to reflect the relative importance of the objective functions in the optimization.

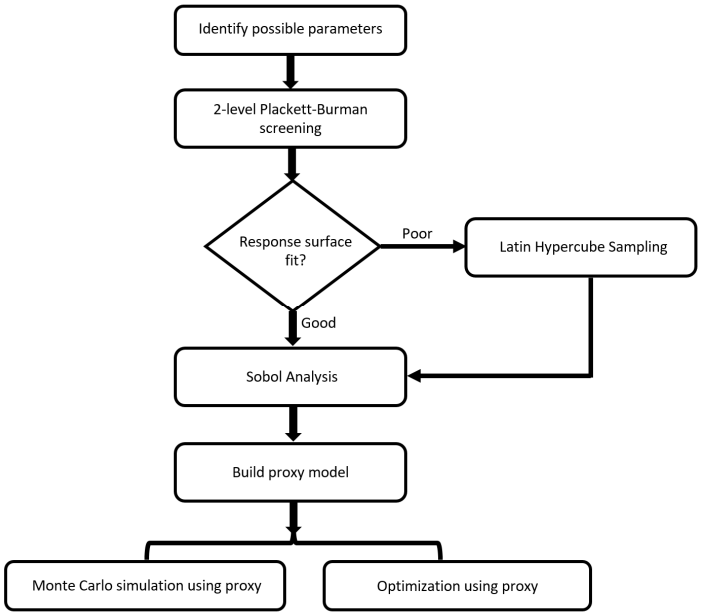

Figure 3. General DoE framework implemented in this study.

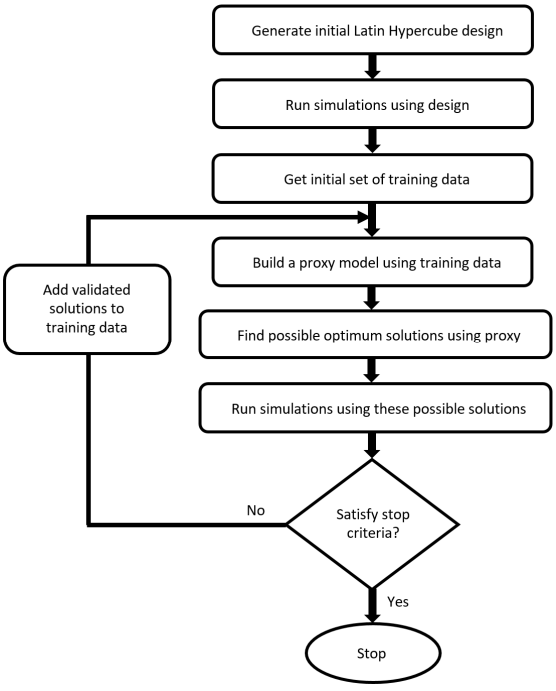

Figure 4. Optimization algorithm in Latin Hypercube plus proxy optimization (adapted from [50]).

5. Results and Discussion

5.1. Simulator Validation

Prior to conducting multi-dimensional simulations, we performed controlled calibration and verification of the simulator used to identify and assess the key governing mechanism related to CO_2-EGR and storage. These mechanisms were studied to ensure the accuracy and representativeness of our simulation models. The investigated mechanisms include:

- CO_2 solubility in water as a function of pressure, temperature, and salinity.
- CO_2 density (molar volume) as a function of pressure and temperature.
- CO_2-saturated water density as a function of pressure and temperature.
- Water vaporization as a function of pressure and temperature.

The solubility of CO_2 in pure water versus pressure and temperature is shown in Figure 5. CO_2 solubility increases with increasing pressure and decreases with increasing temperature. The simulator calculates the fugacity of gas components soluble in the aqueous phase using Henry's law [43], as previously discussed. There is a good match between the experimental data and the calculations for the range of data presented. The model is also capable of calculating CO_2 solubility in water at different salinities (see Figure 6), where the method based on the Scaled Particle Theory by Li and Nghiem [51] is used to correct Henry's constants in the presence of salt.

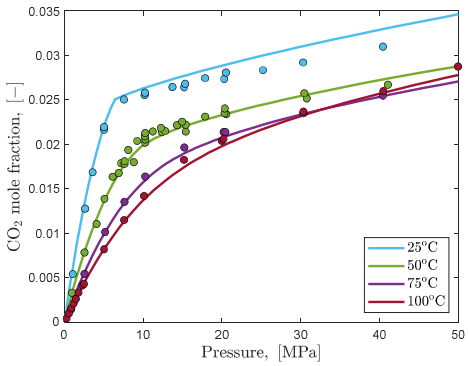

Figure 5. Solubility of CO_2 in pure water as a function of pressure and temperature. The discrete points represent experimental data from [52], and the continuous lines are calculated by the simulator.

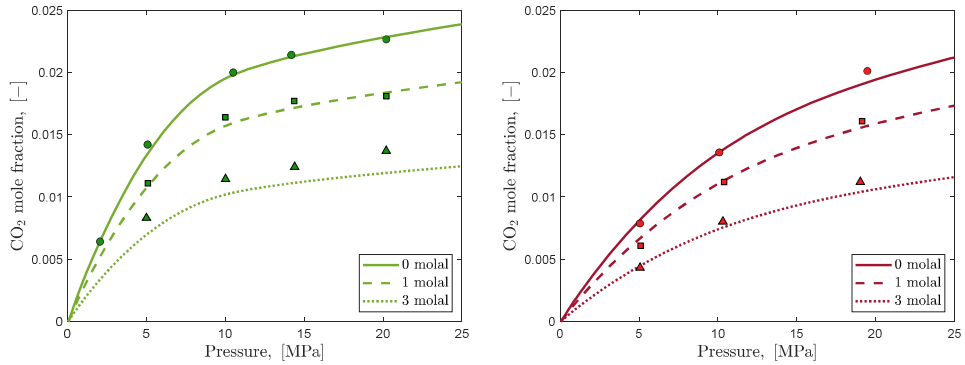

Figure 6. Solubility of CO_2 in 0, 1, and 3 molal brine at 50 °C (left) and 100 °C (right) as a function of pressure. The discrete points are experimental data presented in [53], and the continuous lines are calculated by the simulator.

The density of the gaseous phase is calculated using the Peng-Robinson correlation [42]. Figure 7 shows excellent agreement between the calculated density of CO_2, related to the molar volume by molar mass, and the experimental data for a range of pressures and temperatures. The density of the aqueous phase considering dissolved components is calculated using the Rowe-Chou correlation [54]. Figure 8 shows the density of the CO_2-saturated aqueous phase as a function of temperature and pressure. The aqueous density increases with increasing pressure and decreases with increasing temperature.

Water vaporization enables the mobilization of previously immobile water at low saturations, which could lead to salt precipitation [55,56]. The water content in the CO_2-rich gas phase as a function of temperature and pressure is shown in Figure 9, with a good match between the calculations and the experimental data.

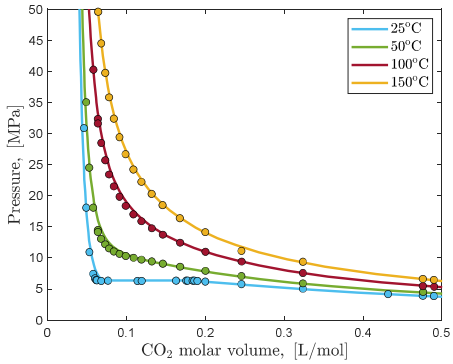

Figure 7. Molar volume of CO_2 as a function of temperature and pressure. The discrete points are experimental data presented in [52], and the continuous lines are calculated by the simulator.

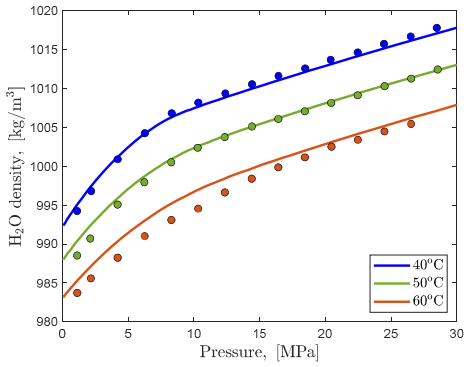

Figure 8. Density of CO_2-saturated water as a function of temperature and pressure. The discrete points are experimental data presented in [57], and the continuous lines are calculated by the simulator.

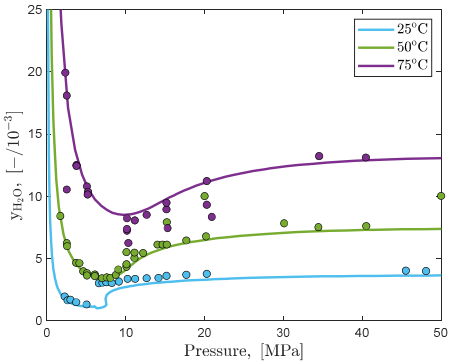

Figure 9. Mole fraction of water in the CO_2-rich gas phase in a water-CO_2 mixture as a function of temperature and pressure. The discrete points are experimental data from [52], and the continuous lines are calculated by the simulator.

5.2. Benefit of Carbonated Water Injection

We performed mechanistic simulations to assess the feasibility of the proposed EGR method, including sensitivity analysis to quantify the uncertainty and identify the optimum transition and operation conditions. Each simulation covers four main periods. First, natural depletion followed by carbonated water injection when the reservoir pressure drops to a certain depletion pressure limit. After a defined volume of carbonated water is injected, pure CO_2 injection follows. Once the reservoir pressure reaches the original reservoir pressure, injection is stopped.

Before carrying out a detailed sensitivity analysis, uncertainty assessment, and optimization, we compared two baseline cases to observe the difference between EGR that

begins with pure CO_2 injection and injection of a slug of carbonated water first. We observe the flow patterns in the 2D cross-sections comparing the two cases, as shown in Figure 10.

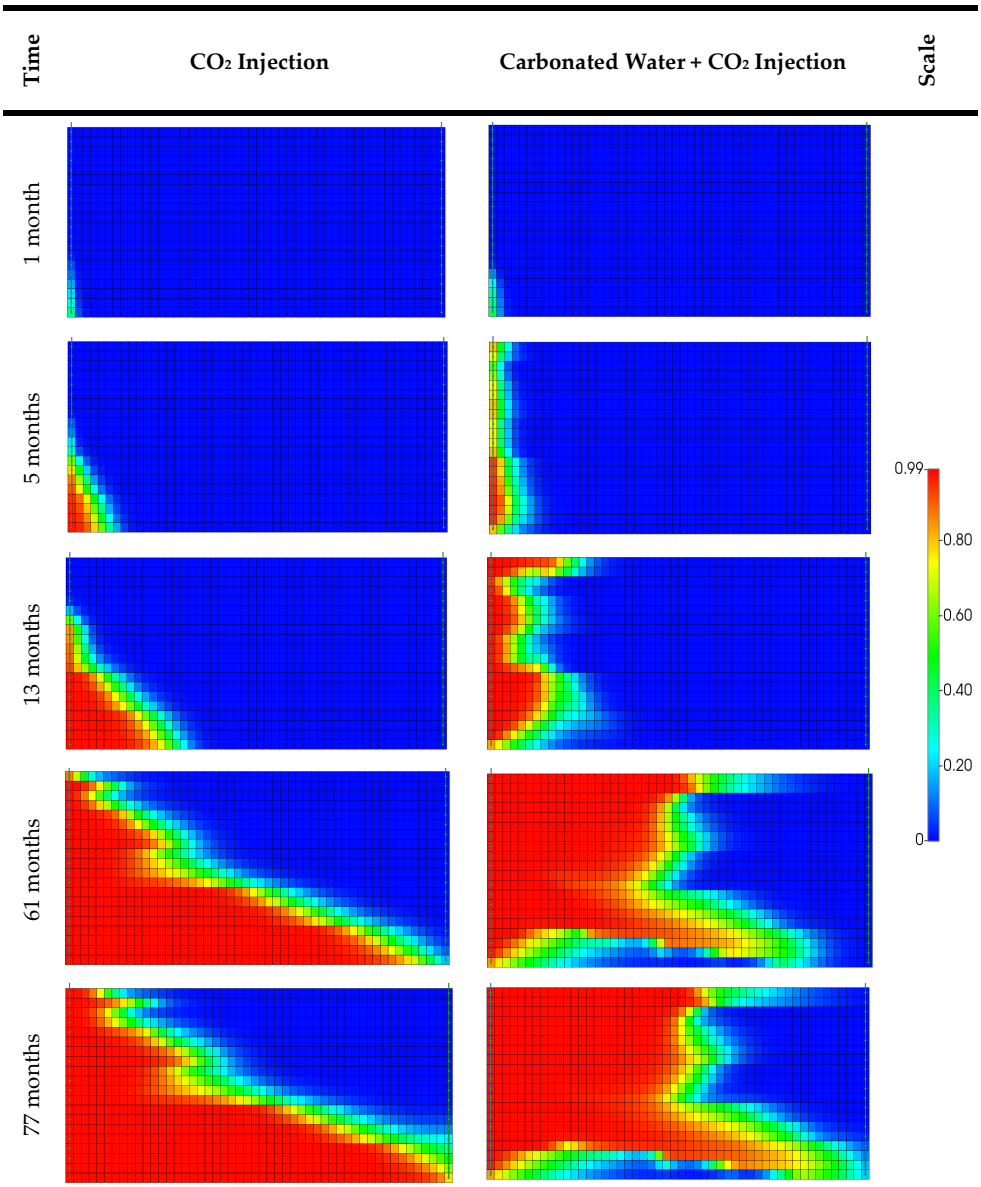

Figure 10. Overall CO_2 mole fraction at different times for CO_2 injection only (left) and carbonated water combined with CO_2 injection (right). The time is given in months since injection began.

Figure 10 shows a series of concentration maps comparing the flow and sweep patterns of the case of CO_2 injection only and the hybrid case of carbonated water combined with CO_2 injection. CO_2 injection and carbonated water injection begin in their respective cases. After 5 months, better sweep and displacement efficiency can be seen in the hybrid case. In the hybrid case, the high permeability channels contain water which inhibits the mobility of CO_2 through these channels, unlike in the absence of carbonated water injection. After 13 months, the injection of the pre-determined carbonated water slug is completed, and the hybrid case switches to pure CO_2 injection. At 61 months, CO_2 breaks through at the production well in the case with no carbonated water slug injected. Comparatively, CO_2 breaks through after 77 months in the hybrid case.

To understand the effect of the volume of carbonated water injected, we performed several simulations with different slug volumes injected from 0 up to 0.1 pore volumes. We compare these cases by the recovery factor, CO_2 stored, and the number of pore volumes

injected at the breakthrough time, which is a direct dimensionless indicator of breakthrough time, as shown in Figure 11. The recovery factor slightly improves as more carbonated water is injected. This behavior is attributed to the lower mobility of water, thus giving a better displacement efficiency. However, the CO_2 stored decreases if more carbonated water is injected, which is attributed to carbonated water occupying potential storage space in the reservoir. On the other hand, breakthrough is delayed for up to 0.1 PV of carbonated water injected. The delay, however, approaches a plateau as more carbonated water is injected. This points to a decreasing benefit as more water is injected.

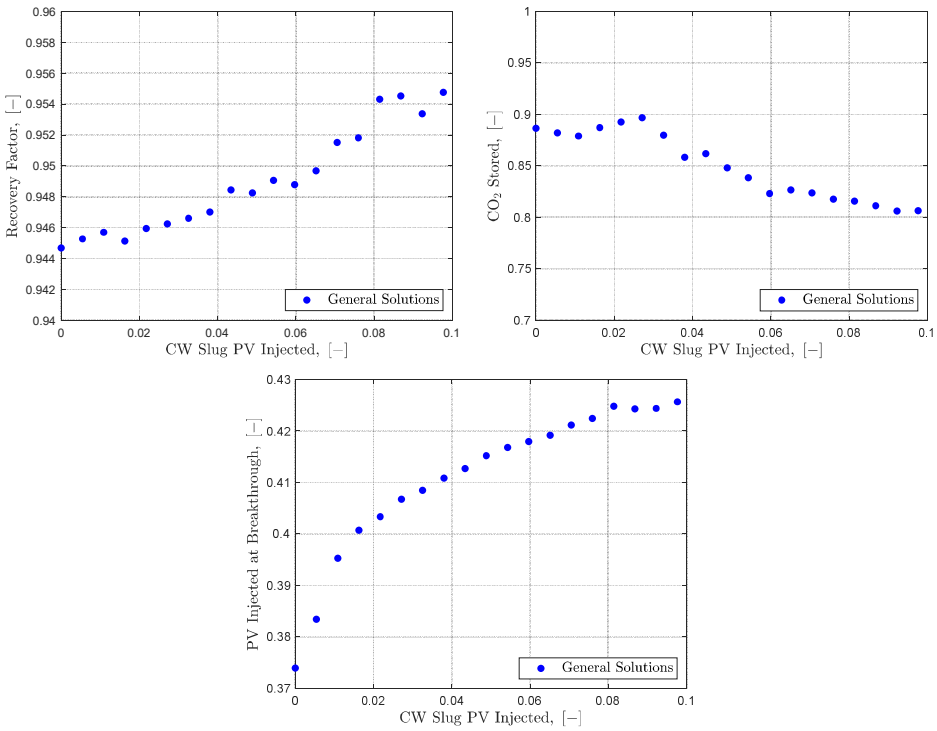

Figure 11. Recovery factor (top left), CO_2 stored (top right), and PV injected at CO_2 breakthrough (bottom) as a function of carbonated water slug volume injected.

Considering the opposing trends observed in Figure 11, we couple these phenomena in a single objective function to quantify the overall benefit of the proposed hybrid scheme. When this objective function is plotted as a function of carbonated water slug volume, we observe an increasing trend followed by a decrease, as shown in Figure 12. This suggests that for up to some amount of carbonated water injected (~0.3 PV in this case), there is a benefit. However, after this amount, there is no evident benefit in injecting a slug of carbonated water considering recovery factor, CO_2 stored, and breakthrough time.

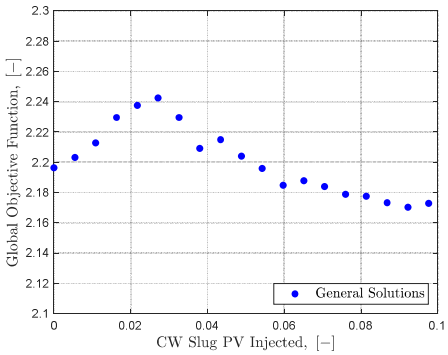

Figure 12. Objective function value as a function of carbonated water slug volume injected.

5.3. Sensitivity Analysis, Uncertainty Assessment, and Optimization

To understand the most dominant parameters influencing the proposed EGR method, we initially performed sensitivity analysis, uncertainty assessment, and optimization on the synthetic cross-section. This study was done following the DoE framework presented in Section 4. The parameters analyzed are presented in Table A1. As part of the sensitivity analysis, the influence of 9 parameters on the methane recovery factor, CO_2 stored, and CO_2 recycled was investigated. The sensitivity was quantified by the Sobol method [49,58], which is a variance-based sensitivity analysis method. About 108 experiments sampled using Latin Hypercube sampling were performed and were sufficient to capture the response surface. The results of the sensitivity analysis are presented in Figure 13, where DP is the Dykstra–Parsons coefficient to quantify heterogeneity, and "EGR Comm. Pressure" is the pressure at which EGR begins.

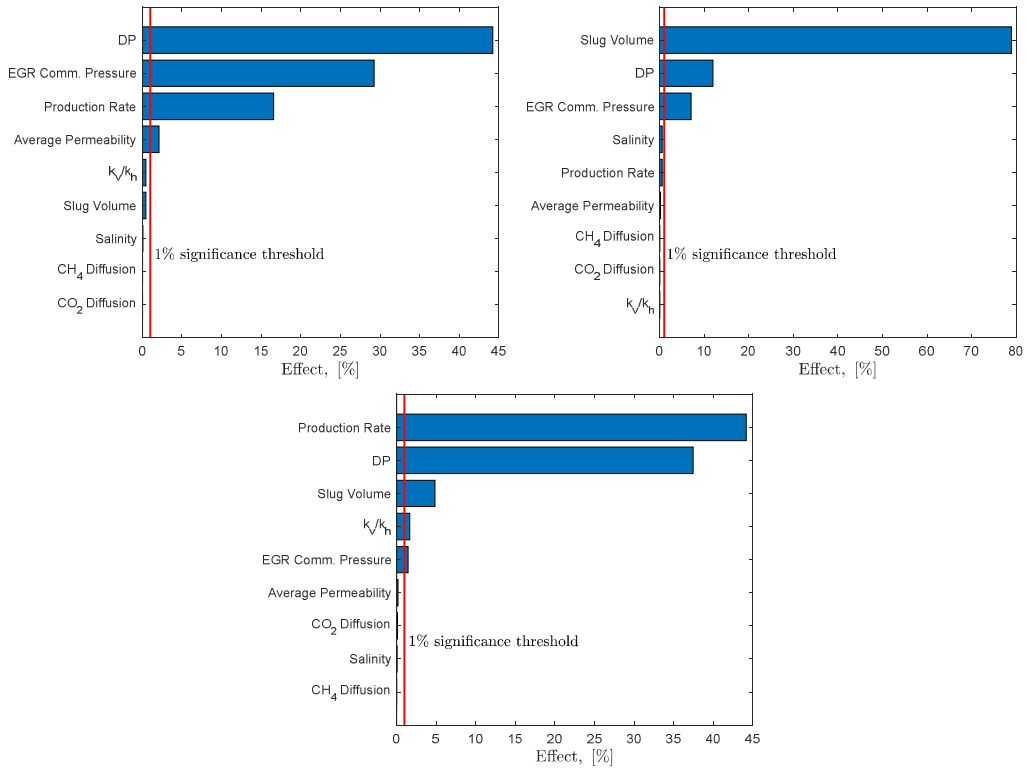

Figure 13. Sobol sensitivity of the influence of 9 parameters on recovery factor (top left), CO_2 stored (top right), and CO_2 recycled (bottom).

A 1% significance threshold was set to eliminate parameters, which did not influence the objective functions. Considering this criterion, parameters chosen for uncertainty assessment are:

- Dykstra–Parsons coefficient;
- Production rate;
- EGR commencement pressure;
- Carbonated water slug volume injected;
- Average permeability;
- Vertical to horizontal permeability ratio.

In the uncertainty quantification, a polynomial proxy model was built using 300 training experiments and verified using 14 blind test cases. Figure 14 shows the proxy verification for the main objective functions; recovery factor, CO_2 stored, and CO_2 recycled. The proxies generated were accurate enough to be used in Monte Carlo simulations, with R^2 values above 0.9.

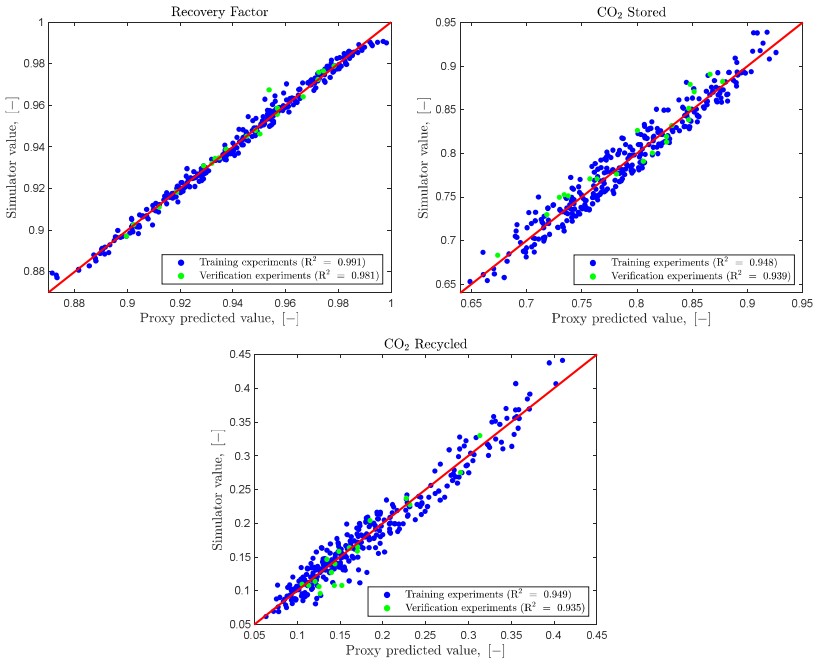

Figure 14. Polynomial proxy verification for recovery factor (top left), CO_2 stored (top right), and CO_2 recycled (bottom).

In the next step, the verified proxy was used for Monte Carlo (MC) simulation. Each MC simulation uses 65,000 samples to ensure few gaps in the sampling space. Better space filling in the sampling space generally gives better predictions [59,60]. The results for methane recovery factor, CO_2 stored, and CO_2 recycled are shown in Figure 15. From the MC simulation, the most likely methane recovery factor is ~94%. This is in agreement with recovery factors from some gas reservoirs around the world, which have reached up to ~96% [61]. The possible recovery factors range between 90% and 98%. The most likely value for CO_2 stored as a percent of the maximum storable CO_2 at the reservoir conditions is ~79%. The range of possible storage ratios is from 71% to 87%. On the other hand, the most likely value for CO_2 recycled is ~16% of the injected CO_2, while the possible range is from 10% to 30%. These results are promising as they show a likelihood of achieving high recovery factors while storing most of the CO_2 injected using the proposed EGR method.

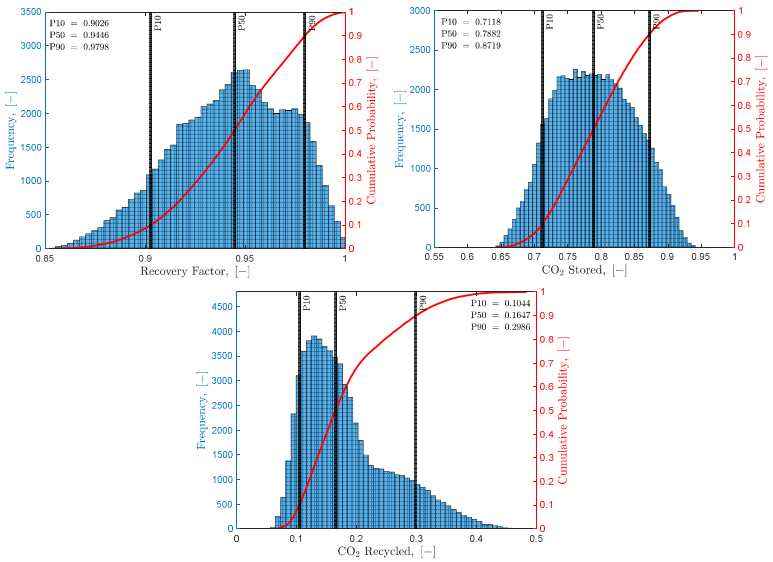

Figure 15. Results from MC simulation showing the recovery factor (top left), CO_2 stored (top right), and CO_2 recycled (bottom) with 65,000 runs.

The polynomial proxy model built was used in the optimization algorithm described in Section 4 to identify the optimum operation and transition conditions for the proposed EGR method. This process is done by maximizing a global objective function that couples the recovery factor, CO_2 stored, and CO_2 recycled. The algorithm analyzes 500 experiments within the optimization framework, as shown in Figure 16.

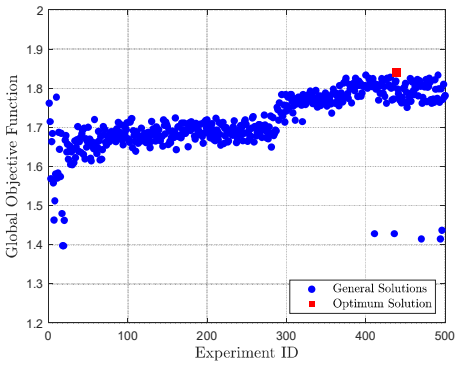

Figure 16. Evolution of the global objective function as the optimization algorithm tries to find an optimum solution.

Initially, a set of experiments is generated by Latin Hypercube sampling and is used to train a proxy model. Once the proxy model is generated, it tries to find an optimum solution, which is validated by a full-physics simulation. In Figure 16, there is a jump in solution quality when the proxy model begins the optimization at ~300 experiments. This result shows the efficiency of the proxy model in finding possible optimum solutions. Some outlier points are the result of the optimizer searching possible far-field solutions to ensure it is not stuck at local maxima.

From the optimization study, the operation and transition conditions of the optimum case were:

- Productivity ratio: 0.5;
- Depletion pressure ratio: 0.115;
- Carbonated water PV injected: 1.5%.

Comparing cases close to the optimum case, we identified that the lower productivity and depletion pressure ratios resulted in the highest global objective function values. In addition, a small PV ranging from 1% to 3% of carbonated water was beneficial. These conditions resulted in the delayed breakthrough of CO_2 and relatively higher methane recovery factors.

5.4. Field Case (Viking Field)

Viking Field is a gas field off the coast of Lincolnshire, England, in the North Sea [62]. It lies in the Rotliegendes sandstone at an approximate depth of 9000 ft subsea [63]. Viking Field has two main reservoirs which are currently depleted, Viking A and Viking B, and several smaller gas pools which totally held approximately 3.6 Tcf of initial gas in place. The produced gas from Viking Field contains 0.3–0.35 mol% of CO_2 [64].

To demonstrate the proposed hybrid EGR method on a more complex multi-dimensional domain, two cases were compared on a sector from the Viking B field. For computational efficiency, the depletion period was omitted, and the initialization reservoir pressure was set to 300 psi, reflecting the actual abundant pressure of the depleted gas reservoir. Figure 17 shows the flow behavior in the sector as CO_2 displaces methane and moves from the injection well to the production well. The wells are placed in a quarter 5-spot pattern. At time zero, injection begins in the respective cases. At 6 months, it is clear how the more mobile CO_2 is advancing faster through the higher permeability layers compared to the carbonated water. At 22 months, carbonated water injection is completed, and pure CO_2 injection begins in the hybrid case. At 129 months, breakthrough occurs in the CO_2-only case,

and the production well is shut-in due to excessive CO_2 production. In comparison, CO_2 breaks through in the hybrid case after 208 months, and the production well is also shut-in.

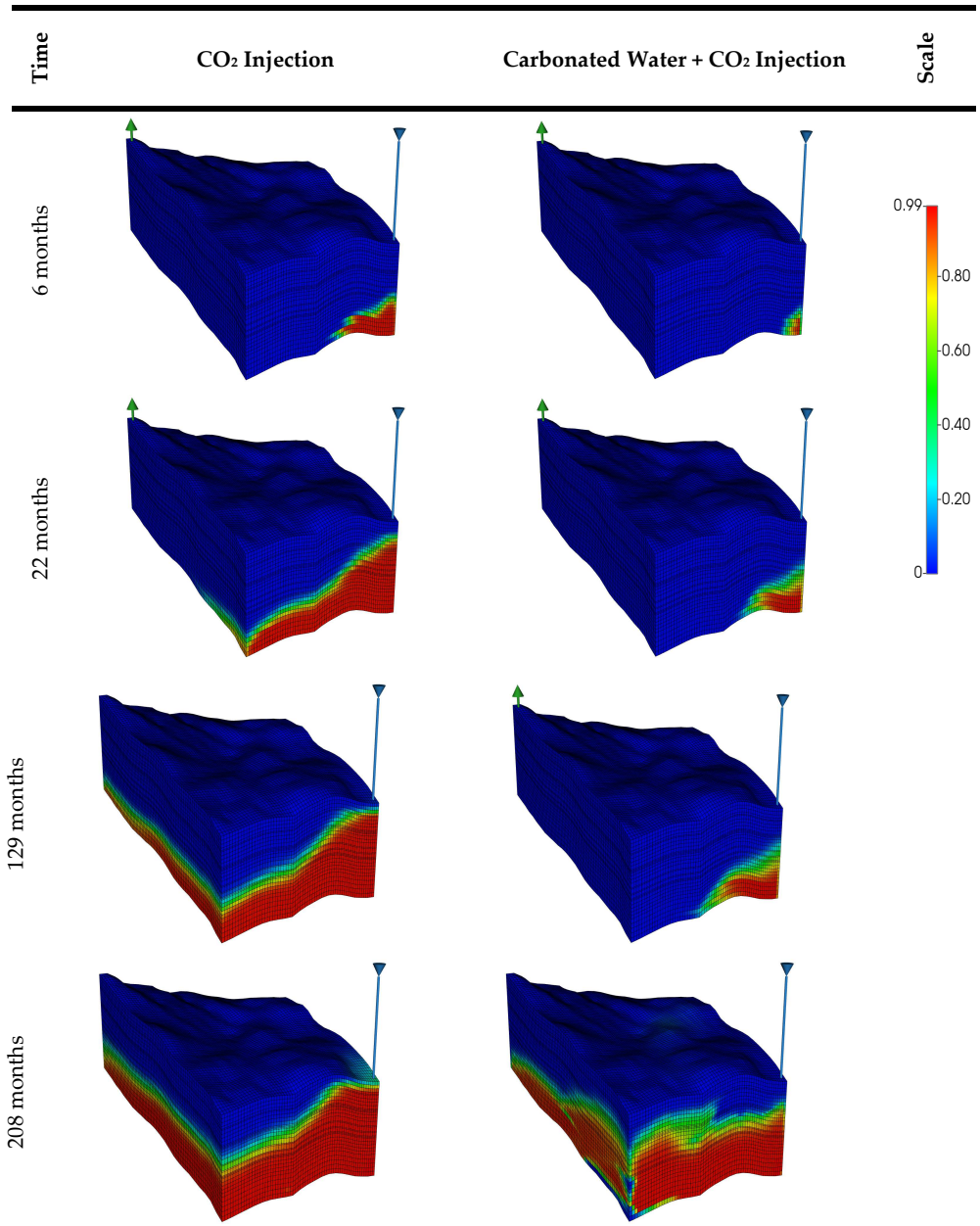

Figure 17. Global CO_2 mole fraction at different times for CO_2 injection only (left) and carbonated water combined with CO_2 injection (right). The time is given in months since injection began.

The above demonstration of flow behavior and breakthrough time on a sector from the Viking Field shows the potential applicability of the proposed hybrid method on more complex multi-dimensional domains. It is, however, important to identify some of the uncertainties associated with scaling up to the field level. The heterogeneity at the field scale is a major source of uncertainty and directly impacts the flow behavior and breakthrough of injected fluids. The available pore volume is also an inherent source of uncertainty, as it affects the available space for CO_2 storage. Furthermore, certain operational and decisional parameters, for instance, well spacing, affect breakthrough and are parameters to be considered in order to optimize the implementation of the method.

5.5. Potential Field Applications, Economics, and Limitations

The proposed hybrid method is very novel and has not been deployed in any actual gas fields as of now. Furthermore, this method has not been previously suggested in published literature, to the best of our knowledge. However, co-injection of carbonated water with supercritical CO_2 for EGR is quite promising, as shown by the presented simulation studies and the field demonstration using a sector from the Viking gas field. Based on published works from the literature, we identify other candidate reservoirs which could potentially benefit from the proposed hybrid method:

- Altmark Field in Germany is a gas field that has reached the tail end of its production phase, with a recovery factor > 78%. The reservoir pressure in the more productive Altensazwedel compartment of this field has dropped to 4000 kPa. Altmark Field has been considered as a candidate for CO_2 EGR coupled with storage, and several studies have been done to investigate the feasibility of this [18,65,66]. The permeability distribution in the Altensazwedel compartment is such that higher permeability layers are lower in the compartment. Studies showed that the CO_2 distribution in the reservoir after injection was strongly linked to the heterogeneity configuration, and breakthrough was likely to occur after ~96 months from the beginning of injection [67].
- K12-B Field is an offshore gas field located in the Dutch sector of the North Sea, which was close to depletion when CO_2 injection field tests were conducted [68,69]. Gas production was from the Rotliegendes formation, with a heterogeneity configuration similar to the Viking Field. Monitoring studies for the CO_2 injection pilot showed CO_2 breakthrough to the production wells after 130 days for the first well and after 463 days for the second well [70].
- Otway CO_2 storage project was the first CCS project implemented in Australia. Natural gas was produced from the Naylor Field, and CO_2 injection was done into a 25–30 m thick sandstone reservoir in this field [71,72]. Monitoring studies showed the injected CO_2 form a plume that migrated up-dip to the production wells through the more permeable layers in the mid-bottom of the reservoir. Tracers injected along with the CO_2 were observed at the production wells after ~150 days, pointing to an early breakthrough [73].

From a technical perspective, the obtained results support the benefit of the hybrid CO_2 injection method. However, for implementation in actual fields, the effectiveness of this method will be determined not only by its technical efficacy but rather by considering the additional benefit it provides in terms of project economics, with or without external incentives. The additional benefit given by the delayed breakthrough and extended production period must be compared against the capital and operation cost of injecting carbonated water. Various potential fields have different infrastructures in place, and the additional cost value may vary significantly depending on the already available facilities and the individual need for upgrades. Therefore, each candidate field must be evaluated individually to weigh the technical benefit of injecting carbonated water against the financial cost of its implementation.

While the proposed hybrid method in this work is promising and shows good potential, it is necessary to highlight some of the limitations or possible challenges that could be encountered while implementing this method. Some of these challenges include:

- The proposed method is dependent on the individual reservoir heterogeneity. Therefore, each case must be individually evaluated in detail to determine whether this method could be applicable and beneficial or not.
- Results have shown that up to 3% PV of injected carbonated water is beneficial. This is a significant amount of water required for injection and could be a challenge for fields that do not have an existing water supply available.
- The preparation of carbonated water in large quantities under desired pressure and temperature conditions may require specialized processing facilities. This could be an additional cost to the overall project expenses.

- The dissolution of CO_2 in water leads to the formation of carbonic acid. Carbonic acid could lead to corrosion of steel tubes that are not corrosion-resistant.

6. Conclusions

In this work, we propose a novel CO_2-based enhanced gas recovery (EGR) method to mitigate the issue of early CO_2 breakthrough and excessive recycling in CO_2 EGR. We use reservoir simulation to assess the feasibility and benefit of this method. We also define a Design of Experiments (DoE) framework to understand the most dominant reservoir and operational parameters affecting the proposed method. This DoE framework is also used to quantify the uncertainty involved and perform optimization to find ideal operation and transition conditions for the proposed method. The most salient conclusions from this work include:

- Injection of a slug of carbonated water followed by CO_2 injection is beneficial to some extent considering three factors; recovery factor, CO_2 stored, and CO_2 breakthrough/recycling. In this study, injection of up to ~3% PV of carbonated water was most beneficial considering all three factors. Injection volumes more than this resulted in no benefit compared to only CO_2 injection.
- The recovery factor was mostly affected by the reservoir heterogeneity, depletion pressure, and production rates. The CO_2 stored was mainly affected by the pore volume of carbonated water injected. This is because injection of any amount of water occupied potential storage space in the reservoir. The CO_2 breakthrough and recycling were primarily affected by the production rates and reservoir heterogeneity as high permeability paths allowed much faster CO_2 breakthrough.
- In general, the proposed hybrid EGR method is significantly influenced by reservoir heterogeneity. Compared to only CO_2 injection, the method performs best in reservoirs with high permeability paths in the bottom layers. For CO_2 floods in gas reservoirs, CO_2 is denser than methane and flows to the bottom of the reservoir due to gravity segregation. When it encounters high permeability paths at the lower layers, it is likely to break through much faster. Injection of carbonated water becomes beneficial in such reservoirs because water, also denser than methane and the in-situ brine, flows down to the bottom of the reservoir. This water plugs the high permeability channels and thus hinders the mobility of CO_2, therefore, delaying breakthrough. This also forces the CO_2 injected after the water to go through lower permeability layers resulting in more even sweep profiles.
- From the Monte Carlo simulations performed, the recovery factor is generally high, and P10, P50, and P90 values fall above 90%. The CO_2 stored ranges between ~70% to ~90% of the maximum storable CO_2 at the reservoir conditions. The CO_2 recycled ranges between ~10% to ~30%. These results are promising and show that with the proposed EGR method, high recovery factors can be achieved while storing most of the CO_2 injected with low recycling rates.
- While the proposed method is promising in terms of improving recovery with high storage ratios, it is necessary to weigh this benefit against the cost of implementing the method. This should be done considering both environmental value and external incentives in order to get an overall quantification of its effectiveness and feasibility.
- Modern reservoir simulators are powerful tools that can contribute to CO_2 storage research advancement. These simulators incorporate many mathematical and empirical models that capture different physical phenomena. However, these models are limited to particular ranges of conditions. It is crucial to first verify and properly calibrate simulation models to ensure representativeness and reliability of results before moving to complex multi-dimensional problems. In this study, we take the time to properly validate the simulator used and carefully select appropriate empirical models to calculate important properties such as CO_2 solubility for the range of expected pressure, temperature, and salinity conditions.

- Careful design of experiments combined with proxy modeling is a useful method to exploit computational resources in an efficient manner. Proxy models, when carefully built and verified, allow us to explore multitudes more scenarios compared to full-physics simulations. Optimal solutions are arrived at much faster with proxy models, and thousands of Monte Carlo simulations can be performed within a fraction of the time taken on reservoir simulators. However, it is crucial to validate the results from proxy models as they are not constrained by physics and sometimes give results that violate fundamental physical relations, for instance, recovery factors greater than 1.

Author Contributions: Conceptualization, V.V. and H.H.; methodology, A.O. and H.H.; software, A.O. and M.A.; validation, A.O., M.A. and H.H.; formal analysis, A.O.; investigation, A.O.; resources, H.H.; data curation, A.O.; writing—original draft preparation, A.O.; writing—review and editing, M.A., V.V. and H.H.; visualization, A.O.; supervision, H.H.; project administration, H.H.; funding acquisition, H.H. All authors have read and agreed to the published version of the manuscript.

Funding: This research received no external funding.

Data Availability Statement: All data and codes used in this research are available upon request from the authors.

Acknowledgments: The authors thank Computer Modelling Group (CMG) Ltd. for providing the academic license of CMG simulators to the King Abdullah University of Science and Technology (KAUST).

Conflicts of Interest: The authors declare no conflict of interest.

Appendix A

Table A1. Reservoir and operation parameters in the synthetic simulation model (values defined as ranges are parameters in the sensitivity analysis and uncertainty assessment).

Parameter	Value/Range	Unit
Original reservoir pressure	20,000	kPa
Reservoir temperature	75	°C
Porosity	0.3	-
Average permeability	50–500	mD
Dykstra-Parsons coefficient	0.5–0.9	-
k_v/k_h	0.1–0.5	-
Initial methane saturation	0.8	-
Irreducible water saturation	0.2	-
Salinity	0–3	molal
Molecular diffusion coefficient (aq)	$0–1 \times 10^{-5}$	cm^2/s
CO_2 injection rate	10	% PV/year
Carbonated water slug volume	0–20	% PV
Productivity ratio	0.5–1.5	-
Depletion pressure ratio	0.1–0.25	-

Table A2. Simulation constraints for the synthetic reservoir model.

Constraint	Value	Unit
Simulation time	100	years
Minimum allowed producer bottom hole pressure (BHP)	2000	kPa
Maximum allowed injector BHP	20,000	kPa
Maximum allowed CO_2 cut in production stream	50	%

Table A3. Reservoir and operational parameters for the 3D sector.

Parameter	Value/Range	Unit
Original reservoir pressure	3000	psi
Reservoir temperature	75	°C
k_v/k_h	0.2	-
Initial methane saturation	0.8	-
Irreducible water saturation	0.2	-
Salinity	1	molal
Molecular diffusion coefficient (aq)	1×10^{-5}	cm^2/s
CO_2 injection rate	4	% PV/year
Carbonated water slug volume	2	% PV
Productivity ratio	0.25	-
Depletion pressure ratio	0.1	-

Table A4. Simulation constraints for the 3D reservoir sector.

Constraint	Value	Unit
Simulation time	100	years
Minimum allowed producer bottom hole pressure (BHP)	300	psi
Maximum allowed injector BHP	3000	psi
Maximum allowed CO_2 cut in production stream	50	%

References

1. IEA. *Global Energy Review 2021*; IEA: Paris, France, 2021.
2. EIA. Global Electricity Consumption Continues to Rise Faster Than Population; Today in Energy: 2020. Available online: https://www.eia.gov/todayinenergy/detail.php?id=44095 (accessed on 17 August 2021).
3. Martins, F.; Felgueiras, C.; Smitková, M. Fossil fuel energy consumption in European countries. *Energy Procedia* **2018**, *153*, 107–111. [CrossRef]
4. Covert, T.; Greenstone, M.; Knittel, C.R. Will We Ever Stop Using Fossil Fuels? *J. Econ. Perspect.* **2016**, *30*, 117–138. [CrossRef]
5. Abas, N.; Kalair, A.; Khan, N. Review of fossil fuels and future energy technologies. *Futures* **2015**, *69*, 31–49. [CrossRef]
6. BP. *Energy Outlook*; BP: London, UK, 2020.
7. BP. *Statistical Review of World Energy*; BP: London, UK, 2020.
8. Walker, S.B.; Van Lanen, D.; Mukherjee, U.; Fowler, M. Greenhouse gas emissions reductions from applications of Power-to-Gas in power generation. *Sustain. Energy Technol. Assess.* **2017**, *20*, 25–32. [CrossRef]
9. Ezekiel, J.; Ebigbo, A.; Adams, B.M.; Saar, M.O. Combining natural gas recovery and CO_2-based geothermal energy extraction for electric power generation. *Appl. Energy* **2020**, *269*, 115012. [CrossRef]
10. Al-Shayji, K.; Aleisa, E. Characterizing the fossil fuel impacts in water desalination plants in Kuwait: A Life Cycle Assessment approach. *Energy* **2018**, *158*, 681–692. [CrossRef]
11. Turta, A.; Sim, S.; Singhal, A.; Hawkins, B. Basic Investigations on Enhanced Gas Recovery by Gas-Gas Displacement. *J. Can. Pet. Technol.* **2008**, *47*. [CrossRef]
12. Oldenburg, C.M.; Pruess, K.; Benson, S.M. Process Modeling of CO_2 Injection into Natural Gas Reservoirs for Carbon Sequestration and Enhanced Gas Recovery. *Energy Fuels* **2001**, *15*, 293–298. [CrossRef]
13. EIA. *Monthly Energy Review*; EIA: Washington, DC, USA, 2021. Available online: https://www.eia.gov/totalenergy/data/monthly/previous.php (accessed on 17 August 2021).
14. IPCC. *IPCC Fifth Assessment Report*; IPCC: Geneva, Switzerland, 2014.
15. Mamora, D.; Seo, J. Enhanced Gas Recovery by Carbon Dioxide Sequestration in Depleted Gas Reservoirs. *OnePetro* **2002**. [CrossRef]
16. Oldenburg, C.M.; Benson, S.M. CO_2 Injection for Enhanced Gas Production and Carbon Sequestration. *OnePetro* **2002**. [CrossRef]
17. Patel, M.J.; May, E.F.; Johns, M.L. High-fidelity reservoir simulations of enhanced gas recovery with supercritical CO_2. *Energy* **2016**, *111*, 548–559. [CrossRef]
18. Gou, Y.; Hou, M.Z.; Liu, H.; Zhou, L.; Were, P. Numerical simulation of carbon dioxide injection for enhanced gas recovery (CO_2-EGR) in Altmark natural gas field. *Acta Geotech.* **2013**, *9*, 49–58. [CrossRef]
19. Polak, S.; Grimstad, A.-A. Reservoir simulation study of CO_2 storage and CO_2 -EGR in the Atzbach–Schwanenstadt gas field in Austria. *Energy Procedia* **2009**, *1*, 2961–2968. [CrossRef]
20. Clemens, T.; Wit, K. CO_2 Enhanced Gas Recovery Studied for an Example Gas Reservoir. *OnePetro* **2002**. [CrossRef]

21. Leeuwenburgh, O.; Neele, F.; Hofstee, C.; Weijermans, P.-J.; Boer, H.; Oosthoek, P.; Lefebvre, A.; Godderij, R.; Gutierrez-Neri, M. Enhanced gas recovery–a potential 'U' for CCUS in The Netherlands. *Energy Procedia* **2014**, *63*, 7809–7820. [CrossRef]
22. Abba, M.; Abbas, A.; Nasr, G.G. Enhanced Gas Recovery by CO_2 Injection and Sequestration: Effect of Connate Water Salinity on Displacement Efficiency. *OnePetro* **2017**. [CrossRef]
23. Omar, A.A.; Addassi, M.; Hoteit, H.; Vahrenkamp, V. A New Enhanced Gas Recovery Scheme Using Carbonated Water and Supercritical CO_2. *SSRN Electron. J.* **2021**, 1–11. [CrossRef]
24. Honari, A.; Hughes, T.J.; Fridjonsson, E.O.; Johns, M.L.; May, E.F. Dispersion of supercritical CO_2 and CH4 in consolidated porous media for enhanced gas recovery simulations. *Int. J. Greenh. Gas Control.* **2013**, *19*, 234–242. [CrossRef]
25. Pooladi-Darvish, M.; Hong, H.; Theys, S.O.P.; Stocker, R.; Bachu, S.; Dashtgard, S. CO_2 Injection for Enhanced Gas Recovery and Geological Storage of CO_2 in the Long Coulee Glauconite F Pool, Alberta. *OnePetro* **2008**. [CrossRef]
26. Hoteit, H.; Fahs, M.; Soltanian, M.R. Assessment of CO_2 Injectivity During Sequestration in Depleted Gas Reservoirs. *Geosciences* **2019**, *9*, 199. [CrossRef]
27. Hoteit, H. Modeling diffusion and gas–oil mass transfer in fractured reservoirs. *J. Pet. Sci. Eng.* **2013**, *105*, 1–17. [CrossRef]
28. Hughes, T.; Honari, A.; Graham, B.F.; Chauhan, A.S.; Johns, M.L.; May, E.F. CO_2 sequestration for enhanced gas recovery: New measurements of supercritical CO_2–CH4 dispersion in porous media and a review of recent research. *Int. J. Greenh. Gas Control.* **2012**, *9*, 457–468. [CrossRef]
29. Blok, K.; Williams, R.; Katofsky, R.; Hendriks, C. Hydrogen production from natural gas, sequestration of recovered CO_2 in depleted gas wells and enhanced natural gas recovery. *Energy* **1997**, *22*, 161–168. [CrossRef]
30. Al-Hasami, A.; Ren, S.; Tohidi, B. CO_2 Injection for Enhanced Gas Recovery and Geo-Storage: Reservoir Simulation and Economics. *OnePetro* **2005**. [CrossRef]
31. Ackerer, P.; Younès, A.; Mancip, M. A new coupling algorithm for density-driven flow in porous media. *Geophys. Res. Lett.* **2004**, *31*. [CrossRef]
32. Shao, Q.; Fahs, M.; Hoteit, H.; Carrera, J.; Ackerer, P.; Younes, A. A 3-D Semianalytical Solution for Density-Driven Flow in Porous Media. *Water Resour. Res.* **2018**, *54*, 10-094–10-116. [CrossRef]
33. Younes, A.; Fahs, M.; Ataie-Ashtiani, B.; Simmons, C.T. Effect of distance-dependent dispersivity on density-driven flow in porous media. *J. Hydrol.* **2020**, *589*, 125204. [CrossRef]
34. Koohbor, B.; Fahs, M.; Ataie-Ashtiani, B.; Belfort, B.; Simmons, C.T.; Younes, A. Uncertainty analysis for seawater intrusion in fractured coastal aquifers: Effects of fracture location, aperture, density and hydrodynamic parameters. *J. Hydrol.* **2019**, *571*, 159–177. [CrossRef]
35. Zhang, W.; Diab, W.; Hajibeygi, H.; Al Kobaisi, M. A Computational Workflow for Flow and Transport in Fractured Porous Media Based on a Hierarchical Nonlinear Discrete Fracture Modeling Approach. *Energies* **2020**, *13*, 6667. [CrossRef]
36. Hoteit, H.; Firoozabadi, A. Numerical Modeling of Diffusion in Fractured Media for Gas-Injection and -Recycling Schemes. *SPE J.* **2009**, *14*, 323–337. [CrossRef]
37. Amin, R.; Sidiq, H.; Kennaird, T.; Van Der Steen, E. Gas–gas experimental interfacial tension measurement. *Fluid Phase Equilibria* **2010**, *295*, 230–236. [CrossRef]
38. Darcy, H.P.G. *Les Fontaines Publiques de la Ville de Dijon. Exposition et Application des Principes à Suivre et des Formules à Employer Dans les Questions de Distribution d'eau, Etc.*; Dalamont, V., Ed.; Dijon, France, 1856.
39. Fick, A. Ueber diffusion. *Ann. Phys.* **1855**, *170*, 59–86. [CrossRef]
40. Cussler, E.L. *Multicomponent Diffusion*; Elsevier: Amsterdam, The Netherlands, 2013; Volume 3.
41. Acs, G.; Doleschall, S.; Farkas, E. General Purpose Compositional Model. *Soc. Pet. Eng. J.* **1985**, *25*, 543–553. [CrossRef]
42. Peng, D.-Y.; Robinson, D.B. A New Two-Constant Equation of State. *Ind. Eng. Chem. Fundam.* **1976**, *15*, 59–64. [CrossRef]
43. Henry, W., III. Experiments on the quantity of gases absorbed by water, at different temperatures, and under different pressures. *Philos. Trans. R. Soc. Lond.* **1803**, *93*, 29–274.
44. Addassi, M.; Omar, A.; Ghorayeb, K.; Hoteit, H. Comparison of various reactive transport simulators for geological carbon sequestration. *Int. J. Greenh. Gas Control.* **2021**, *110*, 103419. [CrossRef]
45. Dykstra, H.; Parsons, R.L. The prediction of oil recovery by waterflood. In *Secondary Recovery of Oil in The United States*; American Petroleum Institute: Washington, DC, USA, 1950; Volume 2, pp. 160–174.
46. Plackett, R.L.; Burman, J.P. The Design of Optimum Multifactorial Experiments. *Biometrika* **1946**, *33*, 305. [CrossRef]
47. Santoso, R.; Torrealba, V.; Hoteit, H. Investigation of an Improved Polymer Flooding Scheme by Compositionally-Tuned Slugs. *Processes* **2020**, *8*, 197. [CrossRef]
48. Santoso, R.K.; Hoteit, H.; Vahrenkamp, V. Optimization of Energy Recovery from Geothermal Reservoirs Undergoing Re-Injection: Conceptual Application in Saudi Arabia. *OnePetro* **2019**. [CrossRef]
49. Sobol, I. Sensitivity Estimates for Nonlinear Mathematical Models. *Mat. Model.* **1993**, *2*, 112–118.
50. CMG. *CMOST: Intelligent Optimization & Analysis Tool*; CMG: Calgary, Canada, 2019.
51. Li, Y.; Nghiem, L.X. Phase equilibria of oil, gas and water/brine mixtures from a cubic equation of state and Henry's law. *Can. J. Chem. Eng.* **1986**, *64*, 486–496. [CrossRef]
52. Appelo, C.; Parkhurst, D.; Post, V. Equations for calculating hydrogeochemical reactions of minerals and gases such as CO_2 at high pressures and temperatures. *Geochim. Cosmochim. Acta* **2014**, *125*, 49–67. [CrossRef]

53. Koschel, D.; Coxam, J.-Y.; Rodier, L.; Majer, V. Enthalpy and solubility data of CO_2 in water and NaCl(aq) at conditions of interest for geological sequestration. *Fluid Phase Equilibria* **2006**, *247*, 107–120. [CrossRef]
54. Rowe, A.M.; Chou, J.C.S. Pressure-volume-temperature-concentration relation of aqueous sodium chloride solutions. *J. Chem. Eng. Data* **1970**, *15*, 61–66. [CrossRef]
55. Miri, R.; Hellevang, H. Salt precipitation during CO_2 storage—A review. *Int. J. Greenh. Gas Control* **2016**, *51*, 136–147. [CrossRef]
56. Tang, Y.; Yang, R.; Kang, X. Modeling the effect of water vaporization and salt precipitation on reservoir properties due to carbon dioxide sequestration in a depleted gas reservoir. *Petroleum* **2018**, *4*, 385–397. [CrossRef]
57. Hebach, A.; Oberhof, A.; Dahmen, N. Density of Water + Carbon Dioxide at Elevated Pressures: Measurements and Correlation. *J. Chem. Eng. Data* **2004**, *49*, 950–953. [CrossRef]
58. Salas, S.; Corrales, M.; Hoteit, H.; Alafifi, A. Quantifying Uncertainty through 3D Geological Modeling for Carbon Capture Utilization and Storage in the Unayzah Formation in Saudi Arabia. *EGU Gen. Assem.* **2021**. [CrossRef]
59. Janssen, H. Monte-Carlo based uncertainty analysis: Sampling efficiency and sampling convergence. *Reliab. Eng. Syst. Saf.* **2013**, *109*, 123–132. [CrossRef]
60. Adepoju, O.O.; Hussein, H.; Chawathe, A. Assessment of Chemical Performance Uncertainty in Chemical EOR Simulations. *OnePetro* **2017**. [CrossRef]
61. Lee, W.J.; Wattenbarger, R.A. *Gas Reservoir Engineering*; Henry L. Doherty Memorial Fund of AIME, Society of Petroleum Engineers: Richardson, TX, USA, 1996; Volume 5.
62. Palmer, J.R.; Tybero, G.; Riches, H.A.; Dudley, G.; Marsh, M.M. Renewed Exploration And Appraisal of the Viking Area: A Case Study. *OnePetro* **1995**. [CrossRef]
63. Gage, M. A Review of the Viking Gas Field. In *Giant Oil and Gas Fields of the Decade 1968–1978*; AAPG: Tulsa, OK, USA, 1980; Volume A012, pp. 39–57.
64. King, W.R.; Taylor, F.R. Field Evaluation of Corrosion Control Chemicals in the Viking Gas Field. *OnePetro* **1975**. [CrossRef]
65. Kuhn, M.; Forster, A.; Großmann, J.; Lillie, J.; Pilz, P.; Reinicke, K.; Schäfer, D.; Tesmer, M. The Altmark Natural Gas Field is prepared for the Enhanced Gas Recovery Pilot Test with CO_2. *Energy Procedia* **2013**, *37*, 6777–6785. [CrossRef]
66. Kühn, M.; Partners, C.; Tesmer, M.; Pilz, P.; Meyer, R.; Reinicke, K.; Förster, A.; Kolditz, O.; Schäfer, D. CLEAN: Project overview on CO_2 large-scale enhanced gas recovery in the Altmark natural gas field (Germany). *Environ. Earth Sci.* **2012**, *67*, 311–321. [CrossRef]
67. Ganzer, L.; Reitenbach, V.; Pudlo, D.; Albrecht, D.; Singhe, A.T.; Awemo, K.N.; Wienand, J.; Gaupp, R. Experimental and numerical investigations on CO_2 injection and enhanced gas recovery effects in Altmark gas field (Central Germany). *Acta Geotech.* **2013**, *9*, 39–47. [CrossRef]
68. Van Der Meer, L.; Kreft, E.; Geel, C.; Hartman, J. K12-B a Test Site for CO_2 Storage and Enhanced Gas Recovery (SPE94128). In Proceedings of the 67th EAGE Conference & Exhibition, Madrid, Spain, 13–16 June 2005.
69. Vandeweijer, V.; van der Meer, B.; Hofstee, C.; Mulders, F.; D'Hoore, D.; Graven, H. Monitoring the CO_2 injection site: K12-B. *Energy Procedia* **2011**, *4*, 5471–5478. [CrossRef]
70. van der Meer, B.L.G.H.; Arts, R.J.; Geel, C.R.; Hofstee, C.; Winthaegen, P.; Hartman, J.; D'Hoore, D. K12-B: Carbon dioxide injection in a nearly depleted gas field offshore the Netherlands. *AAPG* **2009**, 379–390. [CrossRef]
71. Urosevic, M.; Pevzner, R.; Kepic, A.; Wisman, P.; Shulakova, V.; Sharma, S. Time-lapse seismic monitoring of CO_2 injection into a depleted gas reservoir—Naylor Field, Australia. *Lead. Edge* **2010**, *29*, 164–169. [CrossRef]
72. Urosevic, M.; Pevzner, R.; Shulakova, V.; Kepic, A.; Caspari, E.; Sharma, S. Seismic monitoring of CO_2 injection into a depleted gas reservoir–Otway Basin Pilot Project, Australia. *Energy Procedia* **2011**, *4*, 3550–3557. [CrossRef]
73. Jenkins, C.R.; Cook, P.J.; Ennis-King, J.; Undershultz, J.; Boreham, C.; Dance, T.; de Caritat, P.; Etheridge, D.M.; Freifeld, B.; Hortle, A.; et al. Safe storage and effective monitoring of CO_2 in depleted gas fields. *Proc. Natl. Acad. Sci. USA* **2011**, *109*, E35–E41. [CrossRef]